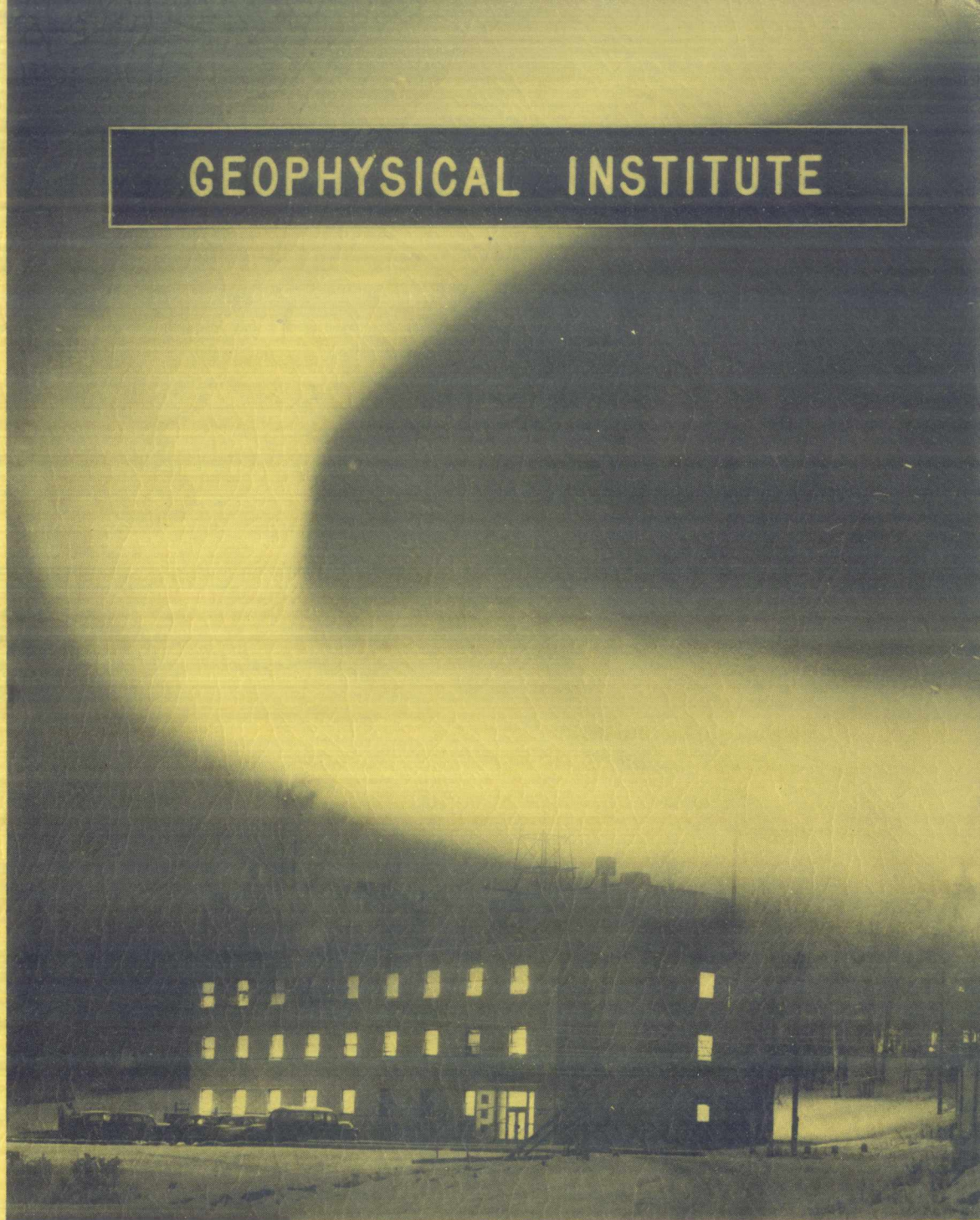


GEOPHYSICAL INSTITUTE

UNIVERSITY
OF ALASKA

COLLEGE
ALASKA

VAG R 74



RADIO PROPERTIES OF THE AURORAL IONOSPHERE

Quarterly Progress Reports Nos. 1-5, 7, 8
1 June 1956 - 31 August 1957
1 December 1957 - 31 May 1958

Air Force Contract No. AF 30(635)-2887
Project No. 5535 - Task 45774

Rome Air Development Center
Griffiss Air Force Base
Rome, New York

GEOPHYSICAL INSTITUTE
of the
UNIVERSITY OF ALASKA

RADIO PROPERTIES OF THE AURORAL IONOSPHERE

Quarterly Progress Reports Nos. 1-5, 7, 8
1 June 1956 - 31 August 1957
1 December 1957 - 31 May 1958

Air Force Contract No. AF 30(635)-2887

Project No. 5535 - Task 45774

Rome Air Development Center, Griffiss Air Force Base

Rome, New York

Report prepared by:

C. Gordon Little
Robert P. Merritt
G. C. Rumi
Ernest Stiltner
Rene Cognard

Report approved by:

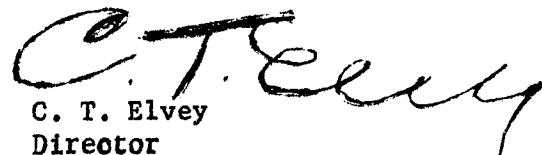

C. T. Elvey
Director

TABLE OF CONTENTS

		Page
ABSTRACT		111
SECTION I	The Phase-Switch Interferometers	1
	Main Parameters of the Equipment	3
	Method of Operation	4
SECTION II	Analysis of Phase-Switch Interferometer Records	7
	Scaling of Records	7
	Probability of Occurrence of Different Indexes of Scintillation Activity	8
	Preparation of Monthly Diurnal Curve of the Mean Value $\frac{\Delta P}{P}$ at 223 Mc.	12
	Preparation of Mean Solar Time and Sidereal Time Variation of Mean $\frac{\Delta P}{P}$ at 223 Mc.	14
	Solar Time Dependence of the Mean Values of $\frac{\Delta P}{P}$ at 223 Mc.	15
	Sidereal Time Dependence of 223 Mc Scintillation Activity	18
	Analysis of Angular Scintillation Information	18
SECTION III	Discussion of Results	23
SECTION IV	Adaptation to an Anisotropic Ionosphere of Booker's Formulae for Radio Star Scintillations	34
SECTION V	Proposed Program of Further Research	50
SUMMARY		51
REFERENCES		53

ERRATA

- Page Line
- 18 5 : Figs 6 and 8
- 35 11 : $n = \left[1 - \frac{Ne^2}{mw^2 \epsilon_0} \right]^{1/2} = 1 - \frac{Ne^2}{2mw^2 \epsilon_0}$
- 19 : mean square deviations are related by the following expression:
- 36 6 : $2c_1$ is the diameter
- 7 : $2a_1$ is the conjugate diameter and $a_2 = a_1 \cos \beta$ is the . . .
- 12 : $\beta = \frac{\pi}{2} - \alpha - \gamma$
- 38 5 : (5)' $= \frac{r_e^2 \lambda^4}{4 \pi^2} \overline{|\Delta N|^2}$
- 9 : (9)' $\frac{1}{D} \overline{|\Delta \phi|^2} = \frac{r_e^2}{2} \lambda^2 c_1 \overline{|\Delta N|^2}$
- 39 1 : (12)' $\overline{|\Delta \phi|^2} = \frac{r_e^2 \lambda^2 \sec \chi}{2} c_1 \overline{|\Delta N|^2}$
- 8 : (19)' $\overline{\theta^2} = 2 \left(\frac{\lambda}{2 \pi a_2} \right)^2 \overline{|\Delta \phi|^2}$
- 9 : (20)' $\overline{\theta^2} = \frac{r_e^2}{4 \pi^2} \lambda^4 \sec \chi \frac{c_1}{a_2} \overline{|\Delta N|^2}$
- 40 8 : (31)' $\overline{\left| \frac{\Delta A}{A} \right|^2} = (2 \pi)^{3/2} r_e^2 \overline{|\Delta N|^2} \dots \dots$
- 41 3 : (37)' $\overline{\left| \frac{\Delta A}{A} \right|^2} = \frac{r_e^2 \lambda^4}{32 \pi^4} \dots \dots$
- 44 1 : $\overline{C_Q} = \left(\frac{E_0 k}{2 \pi D_1 D_2} \right)^2 \dots \dots$
- 7 : = to be deleted.
- 45 2 : $\overline{C_Q} = \left(\frac{E_0 k}{2 \pi D_1 D_2} \right)^2 \dots \dots$
- 5 : $\overline{C_Q} = \left(\frac{E_0 k}{2 \pi D_1 D_2} \right)^2 \dots \dots$
- 46 4 : $\overline{C_Q} = \left(\frac{E_0 k}{2 \pi D_1 D_2} \right)^2 \dots \dots$
- 48 2 : the same as that followed with β and x .
- 8 : ($D_1 = \infty$) becomes

LIST OF FIGURES

Figure		Page
1	Block Diagram of Phase-Switch Interferometer	2
2	Scintillation Index Scaling Limits for 223 Mc	9
3	Scintillation Index Scaling Limits for 456 Mc	10
4	Probability of Occurrence of Scintillation Indexes, 223 Mc and 456 Mc	11
5	Probability Distribution of $\frac{\Delta P}{P}$ for Each Scintillation Index for 223 Mc	13
6	Normalized Solar Time Variation of $\frac{\Delta P}{P}$ for 223 Mc	16
7	Variation of Monthly Median Values of $\frac{\Delta P}{P}$ for 223 Mc	17
8	Solar Time Variation of $\frac{\Delta P}{P}$ for 223 Mc	19
9	Normalized Sidereal Time Variation of $\frac{\Delta P}{P}$	20
10	Normalized Zenith Angle Variation of $\frac{\Delta P}{P}$ for 223 Mc	21
11	Mean Zenith Angle Curves for 223 Mc	22
12	Probability of Occurrence of Angular Scintillation for 223 Mc	25
13	Solar and Sidereal Time Variations of Scintillation Index for 456 Mc	26
14	Zenith Angle Variation of Scintillation Index for 456 Mc	27
15	Diagram of Isotropic and Ellipsoidal Scintillation-causing Irregularities	37
16	Illustration of Complex Correlation Coefficient	49

ABSTRACT

This report, prepared during May 1958, summarizes the analysis of over twelve months of amplitude and angular scintillation data obtained using phase-switch interferometers at 223 Mc and 456 Mc on the Cygnus and Cassiopeia radio sources. The main parameters of the equipment used are first discussed. The method of scaling the records, involving the arbitrary division of the records into four (456 Mc) or six (223 Mc) levels of activity is then described. The probability distributions of the amplitude variations, as derived using a phase-sweep interferometer, are given for the main levels of scintillation activity at 223 Mc. Values of mean fractional deviation of power, $\frac{\overline{\Delta P}}{P}$, for the main levels of activity at 223 Mc are also given. Preliminary probability distributions of angular deviation, and values of mean angular deviation, are also given for the different levels of activity at 223 Mc. The solar-time dependence and sidereal-time (elevation angle) dependence of the scintillation activity are presented and compared with similar data from temperate latitudes. The report concludes with a section in which a recent theory of radio star scintillations⁽⁸⁾ is modified to include the effect of an elongation of the irregularities along the earth's magnetic lines of force.

SECTION I

THE PHASE-SWITCH INTERFEROMETERS

This report is primarily devoted to the analysis of more than one year's data from 223 and 456 Mc phase-switch interferometers. In order to achieve a full understanding of the data and its implications, it is important first to discuss the experimental techniques and operating procedures.

The Equipment

The equipments used are summarized in the block schematic of Fig. 1. Since identical principles are used for either frequency, 223 Mc or 456 Mc, the following discussion will be given for only the 223 Mc channel.

The 223 Mc RF signals from the radio star are picked up on two identical 28 ft. diameter paraboloids and amplified in low noise preamplifiers located in huts below the antennas. Here they are converted to the IF frequency of 32 Mc, using a common crystal-controlled local oscillator signal in order to preserve phase coherence. This oscillator is housed in the central receiving hut, and is fed to the end huts by means of underground coaxial cables. The two 32 Mc IF signals are brought to the central hut, via underground cables, where the phase of one of them is switched through 180 degrees, in a square-wave fashion, at a rate of 1000 times per second. The two IF signals are then mixed, amplified and detected before being passed into an audio amplifier which is tuned to the 1000 cycle phase-reversing frequency.

TABLE I (CONT'D)

Local Oscillator frequency	191.00 Mc (now 255.00 Mc)	424.00 Mc
I F Frequency	32.00 Mc	32.00 Mc
Phase-switching rate	1000 c/s	1100 c/s
Type of phase-switch	Diode switching of quarter-wave-length transmission lines	
Method of Recording	Esterline-Angus 1 ma Pen Recorder	

Method of Operation

During the past year the operation of the phase-switch interferometers has become relatively routine. The standard operational procedure was as follows:

(a) Standard operation

During normal operations, the Esterline-Angus pen recordings of the output of the two phase-switch interferometers were made at 12 inches per hour. At this speed, each roll of chart lasted four days. Throughout this four day period the antennas tracked a single radio star, the antennas being reset at lower culmination each day. At the end of the four day period, the antennas were reset for the other radio star. In this way, each source was observed alternatively for four day periods, and approximately equal quantities of Cygnus and Cassiopeia data were obtained each month. Apart from equipment servicing, the interferometers ran unattended; so far as was possible, continuous 24-hour day, seven-day week operation was sought.

Pen recordings of total power at the output of the main IF of the interferometers were made continuously at a chart speed of 1 inch per hour.

These recordings provided a valuable check on equipment performance, and also served to identify periods of interference.

Hour and minute time marks were placed on the records automatically by means of side pens. In order to ensure minimum pen drag on the phase-switch records, a small 60 cycle ac signal was superimposed on the recording pens.

(b) Daily checks

The zeroes of the DC amplifiers, the balance of the phase sensitive detectors and of the phase switches were checked each day on both equipments. The amplitude of the star signal was adjusted when required so that the peak to peak star signal was about 0.5 of the chart width.

It was necessary to reset the antennas onto the radio star once per day, since the wiring system did not permit continuous rotation in hour angle. The limit stops were set at lower culmination; the hour angles of the antennas were reset each day and made equal to an accuracy of 1/10 of one minute of time, this corresponding to an uncertainty in base-line length of less than 1/10 of one inch. The declination settings were only adjusted each four days, when the antennas were moved to the source. For movements in declination, the antennas were set to equal declinations to an accuracy about two minutes of arc, again introducing a base-line uncertainty of less than 1/10 of one inch. Each time the antennas were reset, time calibrations in Alaska standard time were put on each recorder. Since the records were cut off each day, two complete sets of identification and time marks were made so that both ends of the charts would be fully identified.

(c) Weekly checks

The pen recorders were serviced each week, the ink wells being refilled, and pens washed out. The power supply meters and crystal mixer currents were also checked at this time.

(d) Monthly checks

After some months of operation it was found that a significant amount of observing time was being lost due to equipment failure. At this time a complete tube check, involving over 250 tubes was carried out. This check resulted in the rejection of some 30 weak tubes. Since that date, periodical tube checks have been made approximately every six to eight weeks and have proved very valuable in maintaining the quality and quantity of the data.

Throughout the period the equipment performance was kept under daily surveillance and corrected as required.

SECTION II

ANALYSIS OF RECORDS OBTAINED ON THE PHASE-SWITCH INTERFEROMETERS

Scaling of Records

The output record of the phase-switch interferometer consists of a quasi-sinusoidal trace of slowly varying period, whose amplitude and phase is modulated irregularly by the scintillations of the radio star signal. These records which include both phase and amplitude information are not readily susceptible to exact statistical analysis, primarily owing to the difficulties introduced by the varying periods of the interferometer pattern and the scintillations. Since some 15,000 hours of record had to be analyzed without access to digitizing or machine computing equipment, a simple scaling procedure was required.

The procedure eventually adopted was to divide the records into different levels of activity (indexes of activity) by visual inspection. The different levels of activity were chosen with two points in mind; firstly, it was felt desirable to have roughly equal numbers of records in each group; secondly, an approximately logarithmic scale of activity was found to give levels of activity which could be readily differentiated one from another. It was found possible to divide the 223 Mc data into five main indexes of activity, designated (in increasing order of disturbance) 0, 1, 2, 3, and 4. At 456 Mc, owing to the poorer signal-to-noise ratio and the reduced scintillation activity, it was found possible to divide the records into only three main indexes of activity, namely 0, 1, and 2. An extra index (5 at 223 Mc, 3 at 456 Mc) was used for the recently discovered "fades" of star signal (1).

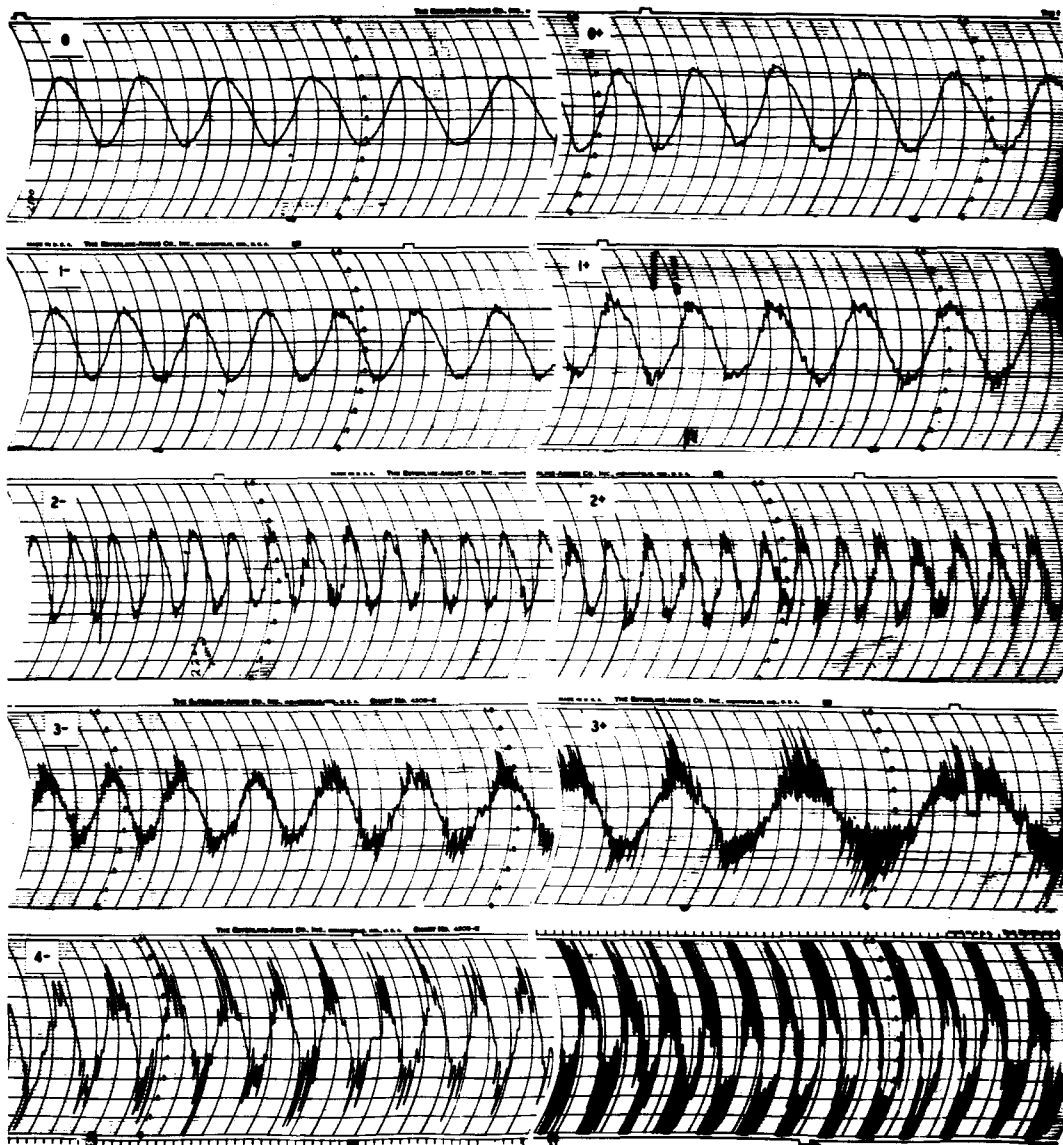
Records showing the limits of activity of each index were selected and photographed (Figs. 2 and 3) to obtain a permanent record of each index suitable for use by the scalars. Experiments showed that, after a little practice, different scalars gave essentially the same index values to a given record, and that scalings carried out at a later date were virtually identical.

Each day's record was marked off into solar hours using 150° West Meridian time and classified into the appropriate index rating. The hourly indexes for a given source and frequency were tabulated and summed for each month to obtain the mean solar time variation of the scintillation index for that particular source, frequency and month.

The mean sidereal time variation for each source, frequency and month was also obtained from the solar time scalings. The continual shift of sidereal time vs solar time of approximately 4 minutes per day was compensated for in a series of steps at intervals of about 15 days. This was done by displacing the data taken in the second half of the month by + 1 hour relative to that taken during the first half, and using the sidereal time appropriate for the seventh or eighth day of the month. In this way, one scaling of the records was used to produce both solar time and sidereal time (elevation angle) diurnal curves for each month.

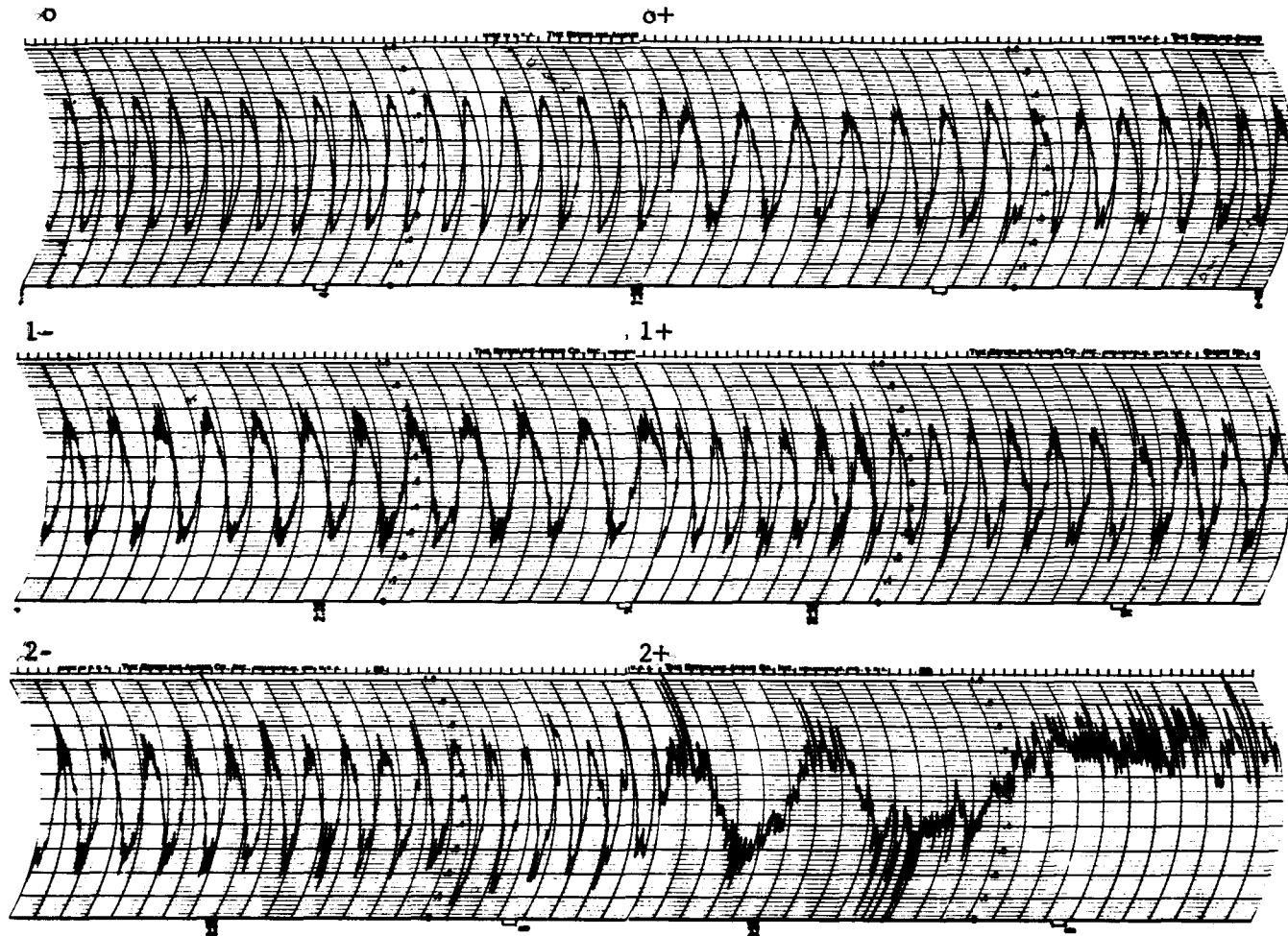
Probability of Occurrence of Different Indexes of Scintillation Activity

The data for the one year period were first analyzed to determine the relative probability of occurrence of each index of scintillation activity. This analysis is summarized in Fig. 4 for each frequency and each source. In general, the scintillation activity at 223 Mc was divided about equally between the five main indexes, 0-4 and less than 1 per cent of the hourly scalings showed significant star fades (index 5).



Scintillation Index Scaling Limits for 223 Mc.

Fig. 2



Scintillation Index Scaling Limits for 456 Mc.

Fig. 3

Preparation of Monthly Diurnal Curves of the Mean Value $\frac{\Delta P}{P}$ at 223 Mc

The scaling of the phase-switch records to hourly indexes of activity has been described above. These indexes, however, have the disadvantage that they do not express the scintillation activity quantitatively. In order to obtain a quantitative figure for the activity, a special series of runs was made on the 223 Mc phase-sweep interferometer (2), for each of the main indexes of activity. These runs were made at a chart speed of 12 inches per minute, simultaneously with the normal phase-switch records. Several lengths of phase-sweep record, each displaying approximately constant scintillation activity, and classified into the appropriate index grouping by means of the phase-switch record, were analyzed to determine the mean value of $\frac{\Delta P}{P}$ and typical probability distribution for each index. The resultant mean values of $\frac{\Delta P}{P}$ and the typical probability distributions for indexes 1, 2, 3, and 4 are given in Fig. 5. Owing to the high level of activity during the period of this special experiment, no observations of index 0 were possible. The probability distribution for index 0 (minimum activity) would be about one half of the width of that for index 1, and it is estimated that the mean value of $\frac{\Delta P}{P}$ (after correction for the residual noise level on the record) would typically be about 0.06.

The mean value of $\frac{\Delta P}{P}$ for each index was then substituted in the monthly tables of hourly scintillation index, to obtain monthly diurnal curves of mean $\frac{\Delta P}{P}$ for each source, in both solar and sidereal time.

Preparation of Mean Solar Time and Sidereal Time Variations of Mean $\frac{\Delta P}{P}$
at 223 Mc

The mean scintillation activity for a given source and frequency may be expected to be a function of season of the year, time of day and of the position of the source in the sky, i.e., of sidereal time. Observations at other northern latitudes have indicated that the seasonal dependence is relatively small, and that the diurnal and elevation angle effects are, to a first order the only ones to be considered. During a period of twelve months, the time at which a given source is seen at a particular elevation angle varies throughout the 24 hours. The (solar) diurnal effect may therefore be determined, free of elevation angle effects, by averaging the data in solar time for one year. Similarly, since a source is always at the same elevation angle at a given sidereal time, the elevation angle effect can be determined, free of diurnal effects, by averaging the data at constant sidereal time for a period of twelve months. These curves may be in error due to possible seasonal effects, (e.g. variation of the diurnal or the elevation dependence with season); however, by using the average diurnal and elevation angle curves determined as above to correct for these two factors it is possible to examine the data in turn for such seasonal trends.

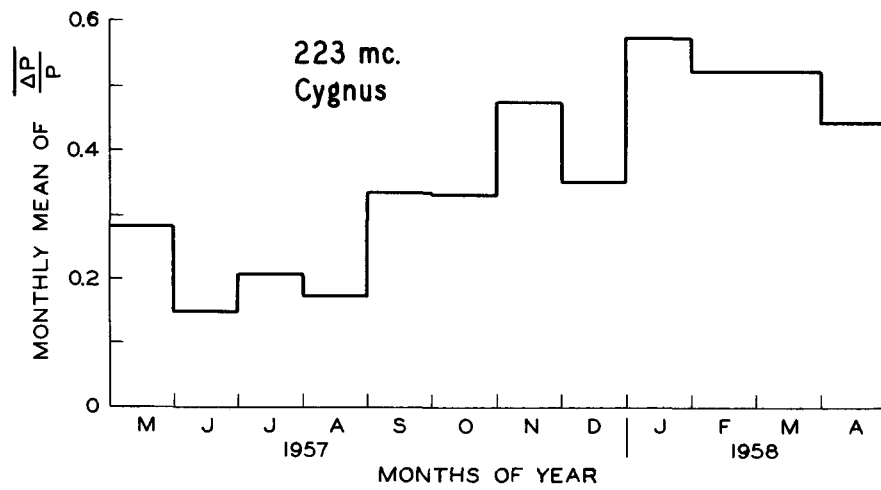
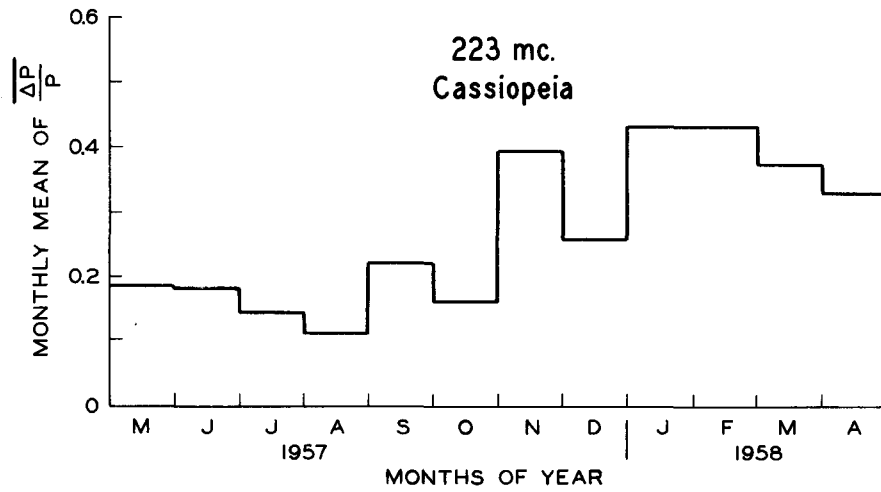
As indicated above, the solar time and sidereal time dependence of radio star scintillations may be separated by averaging twelve successive monthly curves of scintillation activity in solar time or sidereal time respectively. The data for May 1957 through April 1958 were used in this way. Owing to the pressure of observations of the first Soviet Satellite 1957 Alpha-2, limited data were obtained in the following manner.

The diurnal curve obtained in October 1956 was used to give the shape of the curve, and the curve was then normalized to allow for the increase in activity during the year. The normalizing factor was obtained from the mean value of $\frac{\Delta P}{P}$ for the three months October 1956, and September and November 1957, by taking the average value of the ratio September 1957: October 1956 and November 1957: October 1956. In this way, an "October 1957" curve was obtained which is thought to be more satisfactory than that obtained either by using the unnormalized October 1956 data, or an average of the September 1957 and November 1957 data. Since the October data represents only one twelfth of the total data used in preparing the mean annual curves, it is considered that any discrepancies between the true October 1957 curve and the one actually used will have had negligible effect upon the twelve-month averages.

Solar Time Dependence of the Mean Values of $\frac{\Delta P}{P}$ at 223 Mc

Fig. 6 is a plot of the solar time variation of the mean value of $\frac{\Delta P}{P}$ obtained, as described above, by averaging the twelve successive monthly diurnal curves. This curve will be a true representation of the diurnal curve only if the seasonal variation is negligible. Upon examining the mean monthly value of $\frac{\Delta P}{P}$, (Fig. 7), it is apparent the mean scintillation activity varied considerably from month to month during the period from June 1957 to April 1958. No clear evidence of a seasonal trend is apparent, although there is a marked increase in mean activity during the latter portion of the observing period.

In order to minimize the effect of the month-to-month variations in mean activity, the twelve monthly diurnal curves were normalized to obtain diurnal



Variation of Monthly Median Values of $\frac{\Delta P}{P}$ for 223 Mc.

Fig. 7

curves whose mean values were equal. In this way, equal weight was given to the diurnal curve for each month. The twelve normalized, monthly diurnal curves were then summed and averaged to obtain a corrected solar diurnal variation of the scintillation activity at 223 Mc for each source (Fig. 8). The difference between Figs. 7 and 8 is not large, again emphasizing the absence of any large seasonal effects.

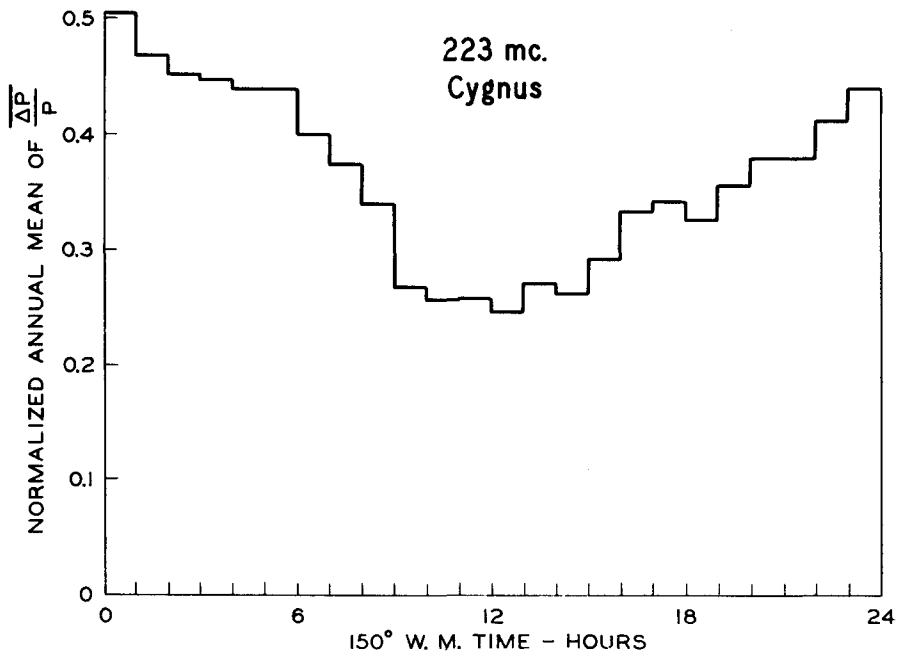
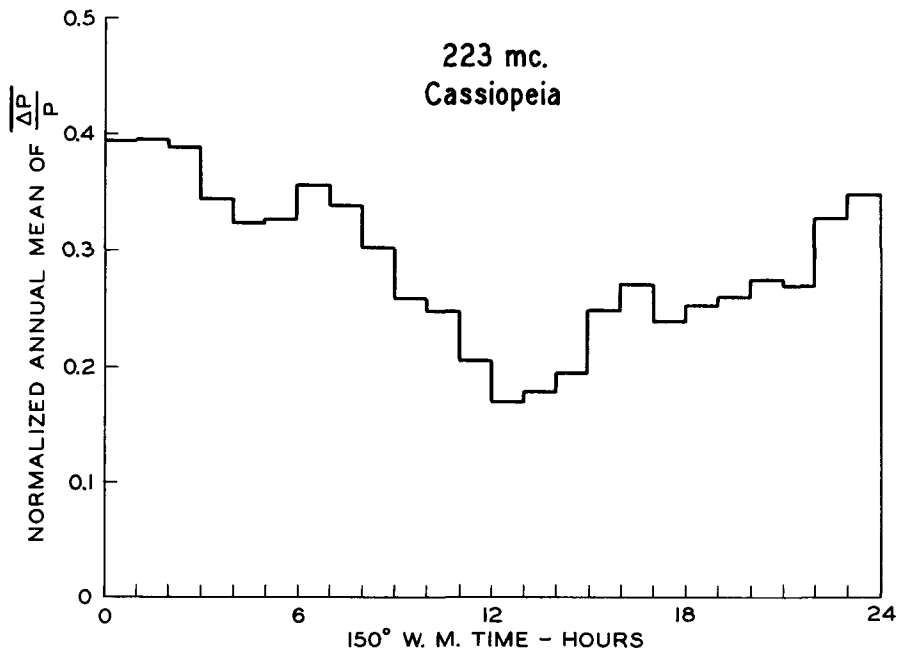
Sidereal Time Dependence of 223 Mc Scintillation Activity

Fig. 9 shows the sidereal time dependence of the 223 Mc scintillation activity for the two sources, obtained in each case as outlined above by averaging twelve consecutive, normalized, monthly diurnal curves in sidereal time. Of greater interest, however, is the elevation angle dependence of the scintillation activity, which may be readily obtained from Fig. 9 since the sidereal time determines the source elevation uniquely.

Fig. 10 shows the elevation angle dependence of the two sources. It will be seen that there appear to be systematic differences in the elevation dependence according to whether the source is rising or setting. This point is discussed further in a succeeding section. The mean elevation angle dependences for each source (obtained by averaging the source rising and setting values) are given in Fig. 11; the interpretation of these curves is also discussed in a succeeding section.

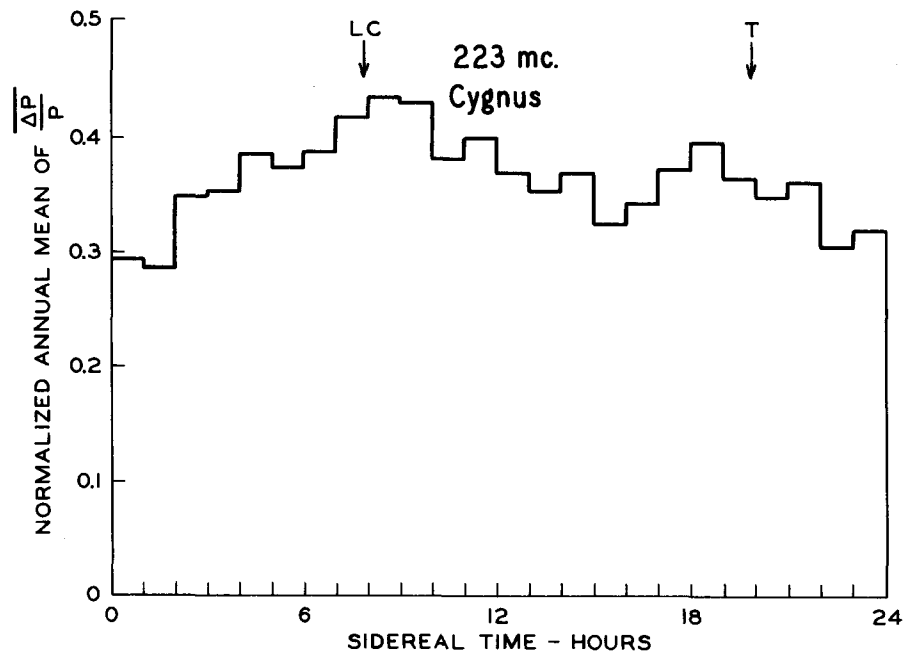
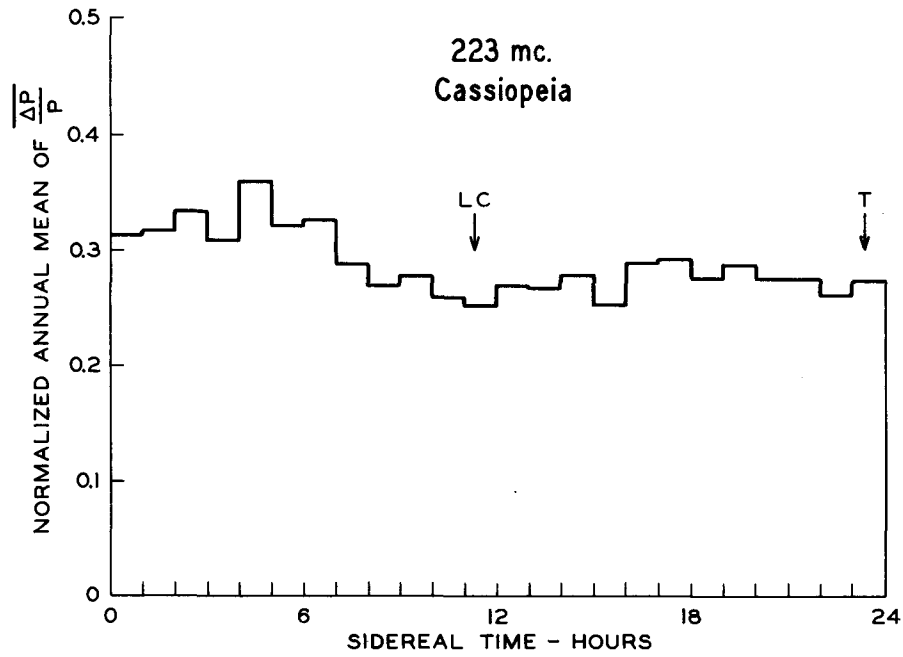
Analysis of Angular Scintillation Information

The times of crossover, or zero crossing, of the phase-switch interferometer output are an accurate measure of the instantaneous angular position of the radio source because at these instants the two IF signals are in phase quadrature. By measuring the times of crossover and noting their deviation



Solar Time Variation of $\frac{\Delta P}{P}$ for 223 Mc.

Fig. 8



Normalized Sidereal Time Variation of $\frac{\Delta P}{P}$ for 223 Mc.

Fig. 9

from the smooth curve defining the motion of a fixed celestial source relative to the lobes of the interferometer, values of angular scintillation can be obtained for each crossover event.

To obtain information on the typical angular scintillation effects occurring during each index of activity, a special series of phase-switch runs were taken. These special runs, taken in addition to the normal phase-sweep records, were made at chart speeds of three inches per minute (vs 12 inches per hour for the routine data) and with a gain approximately three times that of the routine data. The high speed was chosen to allow measurement of the time of occurrence of a crossover event to the nearest second of time, and the gain was such as to drive the recording pen off scale during the peaks of the record and allow an accurate determination of the time of crossover.

The time separation between successive crossover events was read off the record in seconds. A cumulative sum of these values was obtained, starting from an arbitrary point on the record. A value, KN , where K was the mean of the separation between successive crossovers over the period, and N was the number of the crossover as counted from the arbitrary zero, was subtracted from the cumulative sum to obtain a deviation from the constant value K . These values were plotted vs the number of the crossover event and a smooth best-fit curve was drawn through the points. Deviations of the points from the curve were read off to obtain deviations in time for each crossover event. A conversion factor, $d\theta/dt$, was used to convert the deviations in time, Δt , to deviations in angle, $\Delta \theta$.

Fig. 12 gives preliminary curves for the distribution of $\Delta\theta$ for each amplitude scaling index. Later curves, based on further analysis, may show a systematic difference between the mean value of $\Delta\theta$ for a given amplitude index, according to the zenith angle of the source, but are unlikely to affect the curves of Fig. 12 significantly, since they are the average of several transit and lower culmination runs for each index.

456 Mc Data

Owing to the lack of phase-sweep records at 456 Mc, it has not been possible to obtain a mean value of $\frac{\Delta P}{P}$ for the three main indexes of activity at 456 Mc. The solar time variation of the scintillation index for each source, obtained by averaging the monthly diurnal curves of mean index throughout the year, are shown in Fig. 13. The corresponding sidereal time and elevation angle variations of mean index at 456 Mc are given for each source in Figs. 13 and 14. In comparing these data with the 223 Mc data, it is important to remember that the 456 Mc data is inevitably less accurate, owing to the fewer index levels available. Also, the 223 Mc data of Figs. 7 through 12 refer to mean values of $\frac{\Delta P}{P}$, whereas the 456 Mc data refer only to mean scintillation index.

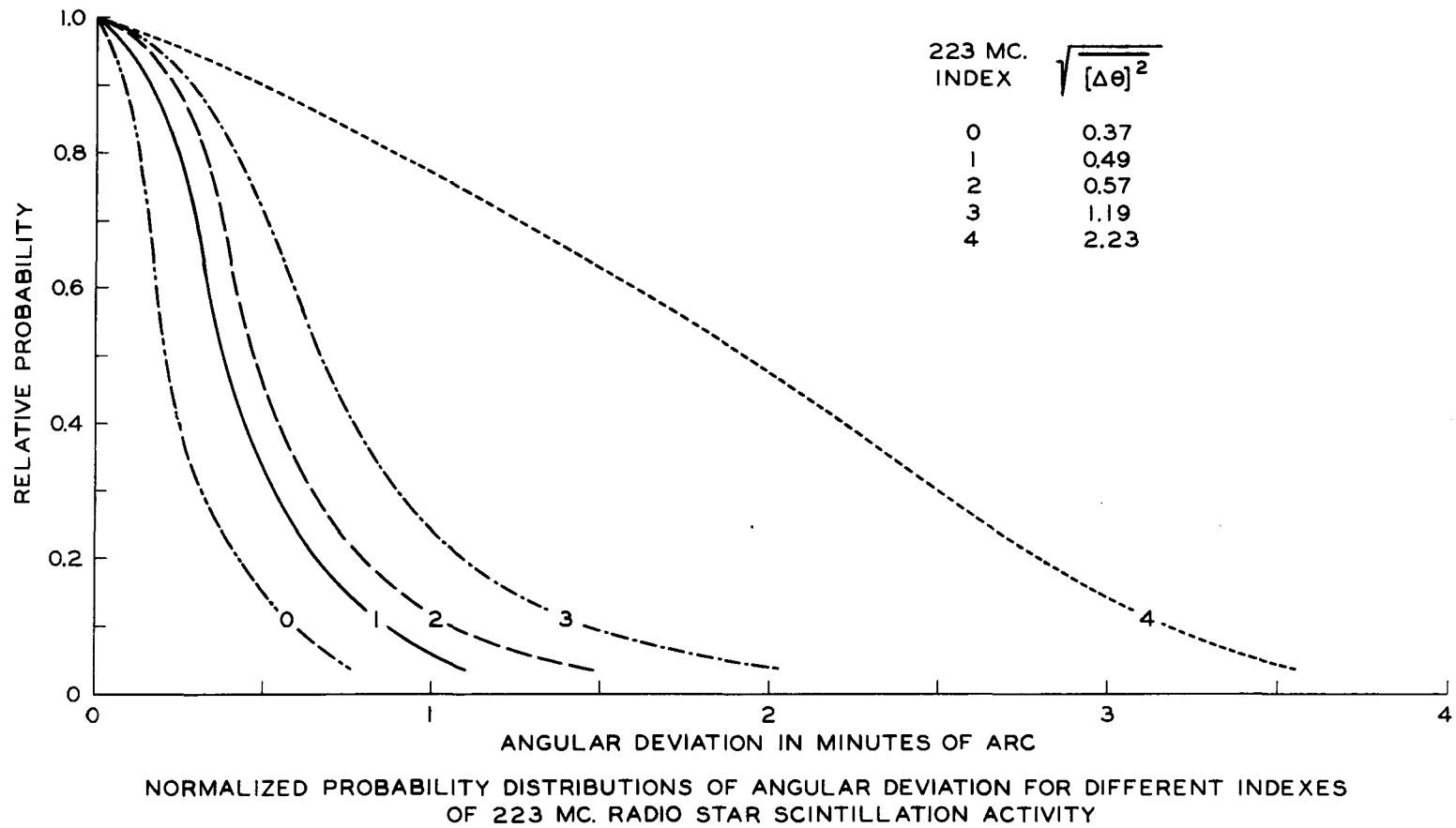


Fig. 12

SECTION III

DISCUSSION OF RESULTS

The Solar Time Variation of Scintillation Activity

Fig. 6 shows that the 223 Mc scintillation activity has a simple diurnal variation with a maximum somewhat after local midnight, and a ratio of about 2:1 between maximum and minimum activity. The following table summarizes a harmonic analysis of the Cygnus and Cassiopeia (solar) diurnal variations in the form

$$\left[\frac{\Delta P}{P} \right] = \sum_{n=0}^4 a_n \sin \left[\frac{2\pi nt}{24} + \sigma_n \right],$$

where n is the harmonic number, t is the local standard time in hours from local midnight (AST plus 9 minutes) and σ_n is the phase angle of the harmonic at local midnight, in degrees.

TABLE 2

Harmonic Analysis of Cygnus and Cassiopeia Diurnal Variation
of Normalized Values of $\left[\frac{\Delta P}{P} \right]$

n	Cygnus		Cassiopeia	
	a_n	σ_n	a_n	σ_n
0	0.363	90	0.287	90
1	0.103	70	0.086	55
2	0.021	322	0.008	300
3	0.013	100	0.031	68
4	0.011	65	0.005	7

It will be seen that the second, third and fourth harmonic terms are very small, and the main variation is in the form of a first harmonic. The mean activity is noticeably greater for Cygnus than for Cassiopeia, (by a ratio of 1.26). This is in part due to the lower mean elevation angle of the Cygnus source, though, as indicated in Fig. 11, there does seem to be a systematic difference between the intensity of the scintillations of the two sources even when viewed at the same elevation angle. The magnitude of the first harmonic relative to the mean component is, however, approximately constant for the two sources, the ratio between the first harmonic and the mean level being 0.283 and 0.298 for the Cygnus and Cassiopeia sources respectively. The phase angles of the first harmonics also agree well, the first harmonics maximizing at 0120 L.S.T. for Cygnus and 0220 L.S.T. for Cassiopeia. These times compare well with the local standard time of magnetic midnight, which, averaged over the year, occurs at about 0150 L.S.T.

In view of the apparent correlation between magnetic midnight and the diurnal maximum of scintillation activity, it is of interest to examine similar data from England. There it was found that the diurnal variation of scintillation activity maximized at about 2300 G.M.T. for the lower culmination of the Cygnus source ⁽³⁾. At these times the F layer of the ionosphere was traversed near the auroral zone. This time again corresponds well to the local magnetic midnight, although it differs from solar time of the College peak by three hours. Recent data for Cassiopeia observations in England by Dagg ⁽⁴⁾ also confirms that the scintillations maximize in amplitude and in rate in England before local midnight. It is difficult to understand why the diurnal curves, if unrelated to magnetic time, should differ in England

and in Alaska and we therefore suggest that the time of maximum activity at any north temperate or auroral latitude is that of local magnetic midnight. This is only one of several evidences of magnetic control of the scintillation activity.

Two important differences between the diurnal variations seen in Alaska and in England are their magnitude and the ratio of the diurnal maximum to minimum. The magnitudes of amplitude scintillation seen by Hewish in England⁽⁵⁾ at 45 Mc indicate that a value of approximately 0.01 for the mean value of $\frac{\Delta P}{P}$ would be expected at 223 Mc. The observed values in Alaska, Fig. 7 are of the order of 0.25, an enhancement of some 25 times.

The diurnal ratio from zenithal observations in England⁽³⁾ showed a very strong variation, in the order of 20 to 1. This value reduced to about 5 to 1 for lower culmination of Cassiopeia (elevation 21 degrees) and less than 2 to 1 for lower culmination of Cygnus (elevation 4 degrees). The diurnal maximum to minimum ratio for College was about 1.3 to 1 for the two sources. These differences between the diurnal variations at different elevation angles and different sites again confirm that the ionospheric disturbing region is a function of latitude, and demonstrates that it shows considerably less diurnal variation at auroral latitudes than at temperate latitudes.

The Elevation Angle Dependence of the 223 Mc Scintillation Activity

An examination of the scintillation vs elevation angle data for the Cygnus source shows that the activity was systematically greater as the source rose from lower culmination than as it approached lower culmination. Such an effect cannot be explained in terms of a simple elevation angle effect, since the elevation angles are symmetrical about lower culmination.

It can, however, be explained qualitatively in terms of a magnetic azimuth effect. Magnetic north is some 30 degrees east of true north at College, and the fact that the Cygnus scintillations maximize at about Hour Angle 14 hours makes it very plausible to suggest that the scintillation activity at low angles of elevation is controlled by magnetic azimuth. This is equivalent to suggesting that the latitude dependence of the disturbing region is a function of geomagnetic rather than geographic latitude.

The probability that the apparent magnetic azimuth effect is a real one is enhanced by comparison with data from Manchester, England. There it was found that the scintillation rates and amplitudes for the Cygnus and Cassiopeia sources maximized about one hour before lower culmination. Since the magnetic declination is about 11 degrees west of true north in England, the peak in the scintillation activity once again corresponds to the direction of geomagnetic north rather than true north. The comparison of two sets of data, one from Alaska and one from England, one maximizing before lower culmination, the other maximizing after lower culmination, but both maximizing towards magnetic north adds weight to the suggestion of a magnetic rather than geographic control of the scintillation activity.

The variation of the mean value of $\frac{\Delta P}{P}$ with the elevation angle, averaged for source rising and setting, is of considerable interest. Booker's theory shows that, for zenith angles not close to 90 degrees, the mean proportionate deviation in amplitude should be proportional to $(\sec \chi)^{3/2}$ where χ is the zenith angle of the source as measured at the ionospheric disturbing layer. The experimental data at College indicates a considerable deviation from the theoretical curve. Whereas the increase of the mean value of $\frac{\Delta A}{A}$ between

transit and lower culmination should have been 4.8 times, the actually observed ratio was only about 1.15. An explanation must therefore be sought for this major discrepancy between theory and practice. A theoretical investigation, now under way, shows that it is probable that this discrepancy can be eliminated, if it is assumed that the irregularities are elongated along the earth's magnetic lines of force. The effect of such an elongation is considered in the next chapter.

Difference Between Scintillation Behavior of the Cygnus and Cassiopeia Sources

Fig. 11 shows that the zenith angle dependence of $\frac{\Delta P}{P}$ for the two sources differ significantly. The Cassiopeia source shows a lower degree of activity, particularly near transit and near lower culmination. The proposed interpretation of this new feature of radio star scintillations lies in the different angular dimensions of the two radio sources. The Cassiopeia source is approximately circular in shape with an angular diameter of approximately 4 minutes of arc.⁽⁶⁾ The Cygnus source, however, is believed to consist of two small objects, each subtending about 1 minute by 0.5 minutes.⁽⁷⁾ The solid angles subtended by the two sources therefore differ by a factor of about twelve. It is suggested that during severe scintillation activity, the different areas of the larger source tend to scintillate independently, with the result that the scintillations are averaged out for the larger source. (This is analogous to the fact that the optical stars scintillate, and that the planets do not.)

With this idea in mind, then, it will be seen that the ratio of Cassiopeia to Cygnus activity will be least when the ratio between the angular subtention of the source and the angular size of the ionospheric irregularities is greatest.

The angular size of a given source is fixed, but the solid angle subtended by the ionospheric irregularities, as viewed from the ground, will be affected both by the distance of the irregularities and, if elongated, by their orientation relative to the line of sight. It is suggested that these two features are the explanation of the discrepancies between the Cygnus and Cassiopeia zenith angle curves, which differ most at transit (when the irregularities are approximately aligned along the line of sight) and at lower culmination, (when the irregularities are furthest from the observer).

SECTION IV

ADAPTATION TO AN ANISOTROPIC IONOSPHERE OF BOOKER'S FORMULAE FOR RADIO STAR SCINTILLATIONS

Booker (8) has presented in the January 1958 issue of Proc. IRE a theory of radio star scintillations, based upon isotropic irregularities in electron density. The following paragraphs describe the modification of the theory to the case where the irregularities are assumed to be ellipsoids of revolution, aligned along the geomagnetic field lines.

We will first comment on the statistical approach of the theory; secondly study in some detail the new geometry to be considered; and then thirdly present the new formulas that take the place of ones presented by Booker. Their application to experimental studies will then be discussed. All formulas are expressed in the M K S system.

Booker, at the beginning of his theory, gives some statistical relations between $\left| \frac{\Delta N}{N} \right|^2$ and $\left| \frac{\Delta n}{n} \right|^2$. It seems appropriate to outline here the approximations involved in these formulae. $\frac{\Delta N}{N}$ and $\frac{\Delta n}{n}$, two random variables expressing the fractional deviation of electron number density and refractive index respectively, are related by an analytical expression that only in first approximation can be reduced either to a linear form or to a quadratic form. The linear approximation is acceptable when the distributions of $\frac{\Delta N}{N}$ and $\frac{\Delta n}{n}$ are concentrated around the mean, i.e., for small deviations of refractive index; the quadratic approximation in the opposite case.

The use of the exact relation between $\frac{\Delta N}{N}$ and $\frac{\Delta n}{n}$, instead of one of the two possible approximations, brings two difficulties. Firstly, one is forced to indicate which one of the two random variables, $\frac{\Delta N}{N}$ and $\frac{\Delta n}{n}$, is independent; indeed the statistical results will vary according to the choice of the independent random variable. Secondly, the use of the exact expression that gives the dependence of $\frac{\Delta n}{n}$ from $\frac{\Delta N}{N}$, or of $\frac{\Delta N}{N}$ from $\frac{\Delta n}{n}$ introduces considerable mathematical complications in the evaluation of

$$\overline{\left| \frac{\Delta n}{n} \right|^2} \text{ or of } \overline{\left| \frac{\Delta N}{N} \right|^2} .$$

In Booker's theory the linear approximation is accepted as valid and the formulas are derived on the basis of the relation

$$n = \left[1 - \frac{Ne^2}{mw^2\epsilon_0} \right] = 1 - \frac{Ne^2}{mw^2\epsilon_0}$$

where e = charge of electron
 m = mass of electron
 ϵ_0 = permittivity of vacuum
 w = angular observing frequency

Therefore, no matter which one is the independent random variable, $\frac{\Delta N}{N}$ and $\frac{\Delta n}{n}$ have probability distributions that differ only by a scaling factor. In our case the scaling factor is $\frac{1}{2} \frac{\lambda^2}{\lambda_N^2 N}$; that means also that the relative mean deviations are related by the following expression:

$$\overline{\left| \frac{\Delta n}{n} \right|^2} = \frac{1}{4} \frac{\lambda^4}{\lambda_N^4 N} \overline{\left| \frac{\Delta N}{N} \right|^2}$$

λ_N = critical wavelength in the layer

With this point clarified we can now proceed to discuss the geometrical considerations required to take into account a possible anisotropy of the irregularities in the ionosphere.

The geometry used by Booker is sketched in Fig. 15a); the geometry we will use is sketched in Fig. 15b).

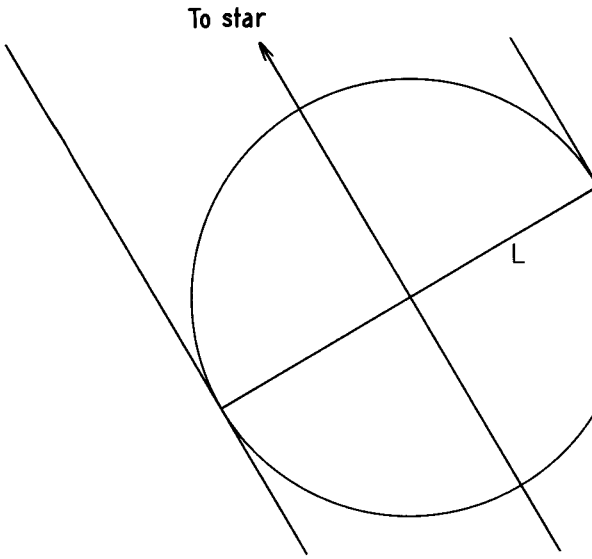
The ellipse in Fig.15 b) is a section of the ellipsoid of correlation in $\frac{\Delta \epsilon}{\epsilon}$, taken in a plane defined by the major axis of the ellipsoid and the direction of the source radiating through the irregular ionosphere. It is assumed that the major axis of the ellipsoid - $2c$ - is aligned with the geomagnetic lines of force. Then γ is the magnetic zenith angle of the source, c_1 is the diameter longitudinal with the direction of the source; a_1 is the conjugate diameter and $a_2 = a_1 \cos \psi$ is the transversal correlation distance to be considered in our problems.

Projective geometry furnishes the relations between these different quantities, namely

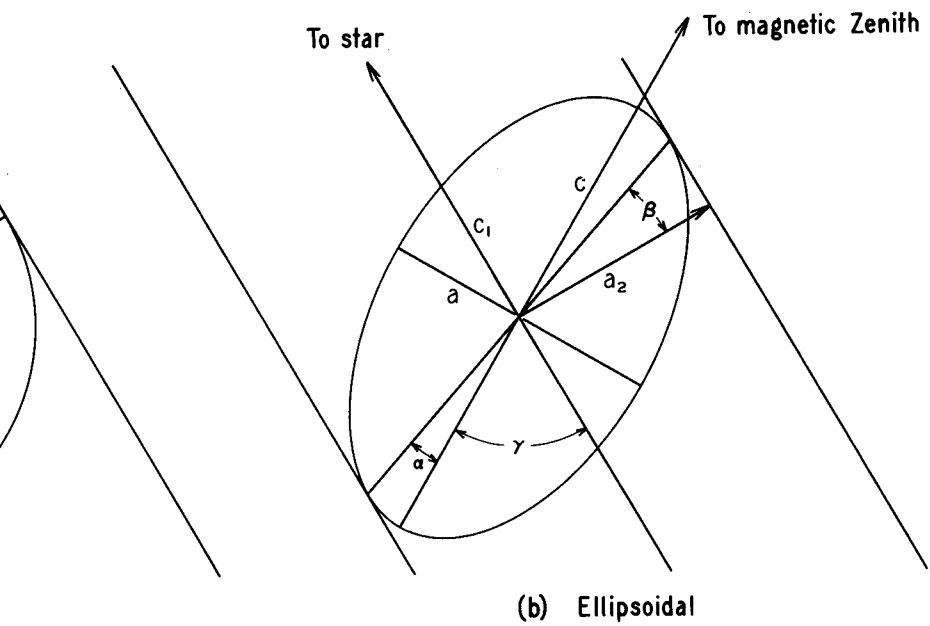
$$\begin{aligned}
 a^2 + c^2 &= a_1^2 + c_1^2 \\
 ac &= a_1 c_1 \sin (\alpha + \gamma) \\
 \frac{c^2}{a^2} &= \tan \alpha \cdot \tan \gamma
 \end{aligned}
 \qquad
 \begin{aligned}
 \alpha &= \frac{\pi}{2} - \alpha - \gamma \\
 (\alpha, \gamma &\text{ acute})
 \end{aligned}$$

The formulas above give the information we require. Indeed for any triplet of data a_1 , c_1 and γ the three unknown a , c , and α can be determined.

With such expressions in mind we can proceed to transform Booker's theory and adapt it in the anisotropic model. We shall transcribe Booker's formula after convenient substitution of c_1 and a_2 to L . The new formulas will be indicated with the same number used by Booker, but marked by an index, for example (1)' instead of (1).



(a) Isotropic



(b) Ellipsoidal

Isotropic and field-aligned irregularities.

$$(1)' \quad \lambda_N^2 = \frac{n}{r_e N}$$

$$(2)' \quad r_e = 2.8 \times 10^{-15} \text{ meters}$$

$$(3)' \quad n^2 = 1 - \frac{\lambda^2}{\lambda_N^2}$$

$$(4)' \quad \overline{\left| \frac{\Delta n}{n} \right|^2} = \frac{\lambda^4}{4 \lambda_N^4} \overline{\left| \frac{\Delta N}{N} \right|^2}$$

$$(5)' \quad = \frac{r_e \lambda^4}{4 \pi^2} \overline{|\Delta N|^2}$$

$$(6)' \quad \left(\frac{2 \pi c_1}{\lambda} \right)^2 \overline{\left| \frac{\Delta n}{n} \right|^2}$$

$$(7)' \quad \frac{D}{2c_1}$$

$$(8)' \quad \overline{|\Delta \phi|^2} = \frac{D}{2c_1} \left(\frac{2 \pi c_1}{\lambda} \right)^2 \overline{\left| \frac{\Delta n}{n} \right|^2}$$

$$(9)' \quad \frac{1}{c_1} \overline{|\Delta \phi|^2} = \frac{r_e^2}{2} \lambda^2 c_1 \overline{|\Delta N|^2}$$

$$(10)' \quad \overline{|\Delta \phi|^2} = \frac{r_e^2 \lambda^2}{2} \int c_1 \overline{|\Delta N|^2} dz$$

$$(11)' \quad \overline{|\Delta \phi|^2} = \frac{r_e^2 \lambda^2}{2} \sec \int c_1 \overline{|\Delta N|^2} dh$$

$$(12)' \quad \overline{|\Delta\phi|^2} = \frac{r_e \lambda^2 \sec}{2} \int c_1 \overline{|\Delta N|^2} \epsilon$$

$$(13)' \quad \overline{|\Delta(\phi_1 - \phi_2)|^2} = 2(1-\rho) \overline{|\Delta\phi|^2}$$

$$(14)' \quad \rho = \exp - \frac{d^2}{a_2^2}$$

$$(15)' \quad \overline{|\Delta(\phi_1 - \phi_2)|^2} = 2 \left(\frac{d}{a_2} \right)^2 \overline{|\Delta\phi|^2}$$

$$(16)' \quad \overline{|\Delta(\phi_1 - \phi_2)|^2} = r_e^2 d^2 \lambda^2 \sec \int \frac{c_1}{a_2^2} \overline{|\Delta N|^2} \epsilon$$

$$(17)' \quad \overline{|\Delta(\phi_1 - \phi_2)|^2} = r_e^2 d^2 \lambda^2 \sec \int \frac{c_1}{a_2^2} \overline{|\Delta N|^2} dh$$

$$(18)' \quad \overline{\theta^2} = \left(\frac{\lambda}{2\pi d} \right)^2 \overline{|\Delta(\phi_1 - \phi_2)|^2}$$

$$(19)' \quad \overline{\theta^2} = 2 \left(\frac{\lambda}{2\pi a_2} \right)^2 \overline{|\Delta\phi|^2}$$

$$(20)' \quad \overline{\theta^2} = \frac{r_e^2}{4\pi^2} \lambda^4 \sec \int \frac{c_1}{a_1^2} \overline{|\Delta N|^2} \epsilon$$

$$(21)' \quad \overline{\theta^2} = \frac{r_e^2}{4\pi^2} \lambda^4 \sec \int \frac{c_1}{a_2^2} \overline{|\Delta N|^2} dh$$

$$(22)' \quad \overline{\left| \frac{\Delta A}{A} \right|^2} = \overline{|\Delta\phi|^2}$$

$$(23)' \quad z_F = \frac{(2\pi a_2)^2}{\lambda}$$

$$(24)' \quad \frac{\lambda}{2\pi a_2}$$

$$(25)' \quad \sigma_F = (2\pi)^{\frac{3}{2}} \pi e \left| \frac{\Delta \epsilon}{\epsilon} \right|^2 \frac{a^2 c}{\lambda^4}$$

$$(26)' \quad \sigma_F = (2\pi)^{\frac{3}{2}} r_e^2 \overline{|\Delta N|^2} a^2 c$$

$$(27)' \quad V = \pi r^2 \left(\frac{\lambda}{2\pi a_2} \right) \sec \chi \left(\frac{\lambda}{2\pi a} \right) \tau$$

$$(28)' \quad P \sigma_F \frac{VS}{r^2}$$

$$(29)' \quad pS$$

$$(30)' \quad \overline{\left| \frac{\Delta A}{A} \right|^2} = \frac{\sigma_F V}{r^2}$$

$$(31)' \quad \overline{\left| \frac{\Delta A}{A} \right|^2} = (2\pi)^{\frac{3}{2}} r_e^2 \overline{|\Delta N|^2} a^2 c \pi \left(\frac{\lambda}{2\pi a_2} \right) \left(\frac{\lambda}{2\pi a} \right) \sec \chi \tau =$$

$$r_e^2 \sqrt{\frac{\pi}{2}} \frac{ac}{a_2} \lambda^2 \sec \chi \tau \overline{|\Delta N|^2}$$

$$(32)' \quad \overline{\left| \frac{\Delta A}{A} \right|^2} = \sqrt{\frac{\pi}{2}} r_e^2 \lambda^2 \sec \chi \int \frac{ac}{a_2} \overline{|\Delta N|^2} dh$$

$$(33)' \quad \overline{\left| \frac{\Delta A}{A} \right|^2} = \left(\frac{z}{z_F} \right)^2 \overline{|\Delta \phi|^2}$$

$$(34)' \quad \overline{\left| \frac{\Delta A}{A} \right|^2} = \frac{z^2 \lambda^2}{(2\pi a_2)^4} \overline{|\Delta \phi|^2}$$

$$(35)' \quad z = h \sec \psi$$

$$(36)' \quad \left| \frac{\Delta A}{A} \right|^2 = \frac{h^2 \lambda^4 \sec^3 \psi r_e^2 c_1}{32\pi^4 a^4} \left| \Delta N \right|^2 \tau$$

$$(37)' \quad \left| \frac{\Delta A}{A} \right|^2 = \frac{r_e^2 \lambda^4}{32\pi^4} \sec^3 \psi \int \frac{h^2 c_1}{a^4} \left| \Delta N \right|^2 dh$$

$$(38)' \quad h = \frac{(2\pi a_2)}{\lambda} a \cos \psi \left\{ \frac{\left| \frac{\Delta A}{A} \right|^2}{\left| \Delta \phi \right|^2} \right\}^{\frac{1}{2}}$$

$$(39)' \quad h = \frac{4\sqrt{2} \pi^2 a_2 d}{\lambda} \cos \psi \left\{ \frac{\left| \frac{\Delta A}{A} \right|^2}{\left| \Delta(\phi_1 - \phi_2) \right|^2} \right\}^{\frac{1}{2}}$$

For the validity of the formulas above, d must be coplanar with the direction of the source and the magnetic zenith direction. For different orientation of d , coefficients that depend from the orientation should be introduced.

Now we will try to see what use we can make of the formulas reported above. We plan to apply the theoretical results with the experimental results one may obtain with a standard interferometer, where the base line, d , is fixed in position on a rotating earth.

Of all the observations produced by an interferometer two are of particular interest, namely, those taken at upper and at lower culmination. For a location, like College, Alaska, at high latitude, field aligned irregularities in the ionosphere are illuminated quasi-longitudinally at the upper culminations and quasi-transversally at the lower culminations of the

Cassiopeia and Cygnus sources. In first approximation we will assume perfect longitudinal or perfect transversal propagation at these times.

With this limitation in mind we take the ratio of different mean square deviations at upper and lower culmination. When the ratio involves both upper and lower culmination, an average of data over a long period, say one year, has to be considered so that the factor $[\Delta N]^2$ can be considered equal at the two positions of the radio star.

TABLE 3

Formulae For Radio Star Scintillation Caused By Ellipsoidal Irregularities Viewed Transversely And Longitudinally

Ratio	Near Screen	Far Screen
$\frac{\left[\frac{\Delta A}{A} \right]_L^2}{\left[\frac{\Delta A}{A} \right]_T^2}$	$\text{Constant} \times \frac{c}{a}$	Constant
$\frac{\left[\Delta(\phi_1 - \phi_2) \right]_L^2}{\left[\Delta(\phi_1 - \phi_2) \right]_T^2}$	$\text{Constant} \times \frac{c}{a}$	$\text{Constant} \times \frac{c}{a}$
$\frac{\left[\frac{\Delta A}{A} \right]_L^2}{\left[\Delta(\phi_1 - \phi_2) \right]_L^2}$	$\text{Constant} \times \frac{1}{a^2}$	$\text{Constant} \times a^2$
$\frac{\left[\frac{\Delta A}{A} \right]_T^2}{\left[\Delta(\phi_1 - \phi_2) \right]_T^2}$	$\text{Constant} \times \frac{1}{a^2}$	$\text{Constant} \times ac$

From the preceding table it is clear that c and a can be measured and a test can be performed to determine whether the screen is at a large or at a close distance with reference to z_F . From an examination of the experimental results, the relative distance of the screen compared to the Fresnel zone distance z_F can be determined for upper and lower culmination.

An alternative and even more efficient way of performing this check is to observe the frequency dependence of $\left| \frac{\Delta A}{A} \right|^2$. (31)' and (36)' indicate that $\left| \frac{\Delta A}{A} \right|^2$ is inversely proportional to the square of the frequency for $z > z_F$, and inversely proportional to the fourth power of the frequency for $z < z_F$.

The ratios C), D), F), and G) imply that phase scintillation is produced at the same level as amplitude scintillation. Equation (39); also makes the same assumption. It is therefore desirable to check this point. One method consists of comparing a measurement of height h through formula (39)' and a second measurement of height which does not require the overlapping of the layers connected with amplitude and phase scintillations. The height of the diffracting screen can be reduced from an expression that gives the complex correlation of signals from radio stars received at two spaced receivers. The general expression of such a correlation for sources not infinitely distant was presented by Feinstein in 1954⁽⁹⁾. This author found that when the source was moved to an infinitely distant point the aspect of the complex correlation function was the same as described by Booker, Ratcliffe and Shinn⁽¹⁰⁾.

A more accurate evaluation of the complex correlation we are speaking about gives different results and leads to different conclusions. The mathematical implications are reported here below: (see Feinstein's⁽⁹⁾ paper for reference).

$$\begin{aligned}
&= \left(\frac{E_0 k}{2\pi D_1 D_2} \right)^B \int_{-\infty}^{\infty} \int_{-\infty}^{\infty} \int_{-\infty}^{\infty} dx \, dx' \, dy \, dy' \cdot e^{\frac{ik}{D} (x-x')^2 + y^2 - y'^2} \\
&\cdot e^{\frac{ik}{D_2} \left\{ s(x+x_0) + v(y+y_0) + x_0 (x-x') + y_0 (y-y') - \frac{s^2}{2} - \frac{v^2}{2} \right\}}
\end{aligned}$$

$$\cdot \frac{1}{2T} \int_{-T}^T dt \cdot e^{i[\Delta\phi(x, y, t) - \Delta\phi(x', y', t)]}$$

$$\frac{1}{D} = \frac{1}{2} \left(\frac{1}{D_1} + \frac{1}{D_2} \right)$$

$$\bar{U}_Q = \left(\frac{E_0 k}{2\pi D_1 D_2} \right) e^{ik(x^2 - x'^2 + y^2 - y'^2)} \iiint_{-\infty}^{\infty} dx dx' dy dy' e^{i(sx_0 + vy_0 - \frac{s^2}{2} - \frac{v^2}{2})}$$

$$e^{i(sx_0 + vy_0 - \frac{s^2}{2} - \frac{v^2}{2})}$$

$$-\frac{1}{2} \phi \Delta \phi \Big|_e (x-x', y-y')$$

Let $\beta = x - x'$ $\gamma = y - y'$

then $d\beta = -dx'$ $d\gamma = -dy'$

$$x - x'^2 = (x+x')(x-x') = (x+x-\beta) \beta = 2x\beta - \beta^2$$

$$= \left(\frac{E_0 k}{2\pi D_1 D_2} \right)^2 \int_{-\infty}^{\infty} \int_{-\infty}^{\infty} dx dy d\beta d\gamma e^{\frac{ik}{D} (2x\beta - \beta^2 + 2y\gamma - \gamma^2)}$$

$$e^{\frac{ik}{D_2} \left\{ sx + vy + x_0 \beta + y_0 \gamma \right\}} e^{\frac{ik}{D_2} \left(sx_0 + vy_0 - \frac{s^2}{2} - \frac{v^2}{2} \right)} e^{-\frac{1}{2} |\Delta \phi|^2 (\beta, \gamma)}$$

$$\frac{1}{D} = \frac{1}{D_2} \left(\frac{1}{2} \frac{D_1 + D_2}{D_1} \right) \quad \frac{1}{D_2} = \frac{1}{D} \frac{2 D_1}{D_1 + D_2}$$

$$= \left(\frac{E_0 k}{2\pi D_1 D_2} \right)^2 \int_{-\infty}^{\infty} \int_{-\infty}^{\infty} dx dy d\beta d\gamma e^{\frac{ik}{D} (2x\beta - \beta^2 + 2y\gamma - \gamma^2)}$$

$$e^{\frac{ik}{D} \frac{2 D_1}{D_1 + D_2} \left\{ sx + vy + x_0 \beta + y_0 \gamma \right\}} e^{\frac{ik}{D_2} \left(sx_0 + vy_0 - \frac{s^2}{2} - \frac{v^2}{2} \right)}$$

$$e^{-\frac{1}{2} |\Delta \phi|^2 (\beta, \gamma)}$$

Fourier integral formula

$$\frac{1}{2} \pi \left\{ f(\delta + 0) + f(\delta - 0) \right\} = \int_0^{\infty} \int_{-\infty}^{\infty} \cos u(t - \delta) f(t) du dt$$

$$\text{Let } u = \frac{2kx}{\bar{D}} \quad t = \beta \quad \delta = \frac{-s D_1}{D_1 + D_2}$$

$$= \left(\frac{E_0 k}{2\pi D_1 D_2} \right)^2 e^{\frac{ik}{D_2} (sx_0 + vy_0 - \frac{s^2}{2} - \frac{v^2}{2})} \int_{-\infty}^{\infty} \int_{-\infty}^{\infty} \int_{-\infty}^{\infty} dy d\gamma dx d\beta$$

$$e^{\frac{i2kx}{\bar{D}} \left(\beta + \frac{s D_1}{D_1 + D_2} \right)} e^{\frac{ik}{\bar{D}} \left(\frac{2x_0 \beta D_1}{D_1 + D_2} - \beta^2 \right)} \text{ similarly in } y \text{ and } \gamma$$

$$e^{-\frac{1}{2} \left| \Delta \phi \right|^2 (\beta, \gamma)}$$

. e

$$= \left(\frac{E_0 k}{2\pi D_1 D_2} \right)^2 e^{\frac{ik}{D_2} (sx_0 + vy_0 - \frac{s^2}{2} - \frac{v^2}{2})} \int_{-\infty}^{\infty} \int_{-\infty}^{\infty} dy d\gamma dt du \left(\frac{\bar{D}}{2k} e^{iu(t - \delta)} \right)$$

$$e^{\frac{ik}{\bar{D}} \left(\frac{2x_0 D_1 t}{D_1 + D_2} - t^2 \right)} \text{ similarly in } y \text{ and } \gamma e^{-\frac{1}{2} \left| \Delta \phi \right|^2 (t, \gamma)}$$

We have that

$$\int_{-\infty}^{\infty} e^{iu(t - \delta)} f(t) du = 2 \int_0^{\infty} \cos u(t - \delta) f(t) du$$

$$\therefore \bar{C}_Q = \left(\frac{E_0 k}{2\pi D_1 D_2} \right)^2 e^{\frac{ik}{D_2} (sx_0 + vy_0 - \frac{s^2}{2} - \frac{v^2}{2})} \int_{-\infty}^{\infty} \int_{-\infty}^{\infty} \int_0^{\infty} dy d\gamma$$

$$dt du \frac{\bar{D}}{k} \cos u(t - \bar{S}) e^{\frac{ik}{\bar{D}} \left(\frac{2x_0 D_1 t}{D_1 + D_2} - t^2 \right)} \text{ similarly in } y \text{ and } \gamma$$

$$e^{-\frac{1}{2} |\Delta\phi|^2} (t, \gamma)$$

$$= \left(\frac{E_0 k}{2\pi D_1 D_2} \right)^2 \frac{\bar{D}}{k} e^{\frac{ik}{D_2} (sx_0 + vy_0 - \frac{s^2}{2} - \frac{v^2}{2})} \iint dy d\gamma e^{\frac{ikx_0}{D_2} \left(-\frac{s D_1}{D_1 + D_2} \right)}$$

$$e^{-\frac{iks^2 D_1}{2D_2 (D_1 + D_2)}} \text{ similarly in } y \text{ and } \gamma e^{-\frac{1}{2} |\Delta\phi|^2} \left(-\frac{s D_1}{D_1 + D_2}, \gamma \right)$$

$$= \left(\frac{E_0 k}{2\pi D_1 D_2} \right)^2 \frac{\bar{D}}{k} \pi e^{\frac{ik}{D_2} \left(sx_0 + vy_0 - \frac{s^2}{2} - \frac{v^2}{2} - \frac{x_0 s D_1}{D_1 + D_2} - \frac{s^2 D_1}{2(D_1 + D_2)} \right)}$$

$$\int_{-\infty}^{\infty} \int_{-\infty}^{\infty} \text{ terms in } y \text{ and } \gamma \cdot e^{-\frac{1}{2} |\Delta\phi|^2} \left(-\frac{s D_1}{D_1 + D_2}, \gamma \right)$$

The procedure to be used with the two remaining integrals is perfectly the same followed with y and x .

$$\begin{aligned} \bar{C}_Q(x_0, y_0; s, v) &= \left(\frac{E_0}{2D_1 D_2} \right)^2 (\bar{D})^2 \cdot e^{\frac{ik}{D_1 + D_2} \left(sx_0 + vy_0 - \frac{s^2}{2} \left(\frac{2D_1 + D_2}{D_2} \right) \right)} \\ &\cdot e^{\frac{ik}{D_1 + D_2} \left(-\frac{v^2}{2} \left(\frac{2D_1 + D_2}{2} \right) \right)} \cdot e^{-\frac{1}{2} \overline{|\Delta \phi|^2} \left(-\frac{s D_1}{D_1 + D_2}, -\frac{v D_1}{D_1 + D_2} \right)} \\ &= \left(\frac{E_0}{D_1 + D_2} \right)^2 \cdot e^{-\frac{1}{2} \overline{|\Delta \phi|^2} \left(-\frac{s D_1}{D_1 + D_2}, -\frac{v D_1}{D_1 + D_2} \right)} \\ &\cdot e^{\frac{ik}{D_1 + D_2} \left[sx_0 + vy_0 - \left(\frac{s^2}{2} + \frac{v^2}{2} \right) \left(\frac{2D_1 + D_2}{D_2} \right) \right]} \end{aligned}$$

The complex correlation function for the case of radio star

($D_1 = D_0$) becomes

$$\bar{C}_Q(x_0, y_0; s, v) = (E_0)^2 \cdot e^{-\frac{1}{2} \overline{|\Delta \phi|^2} (-s, -v)} \cdot e^{-i \frac{k}{D_2} (s^2 + v^2)} \quad (1)$$

A graphical exemplification on Figure 16 illustrates the situation.

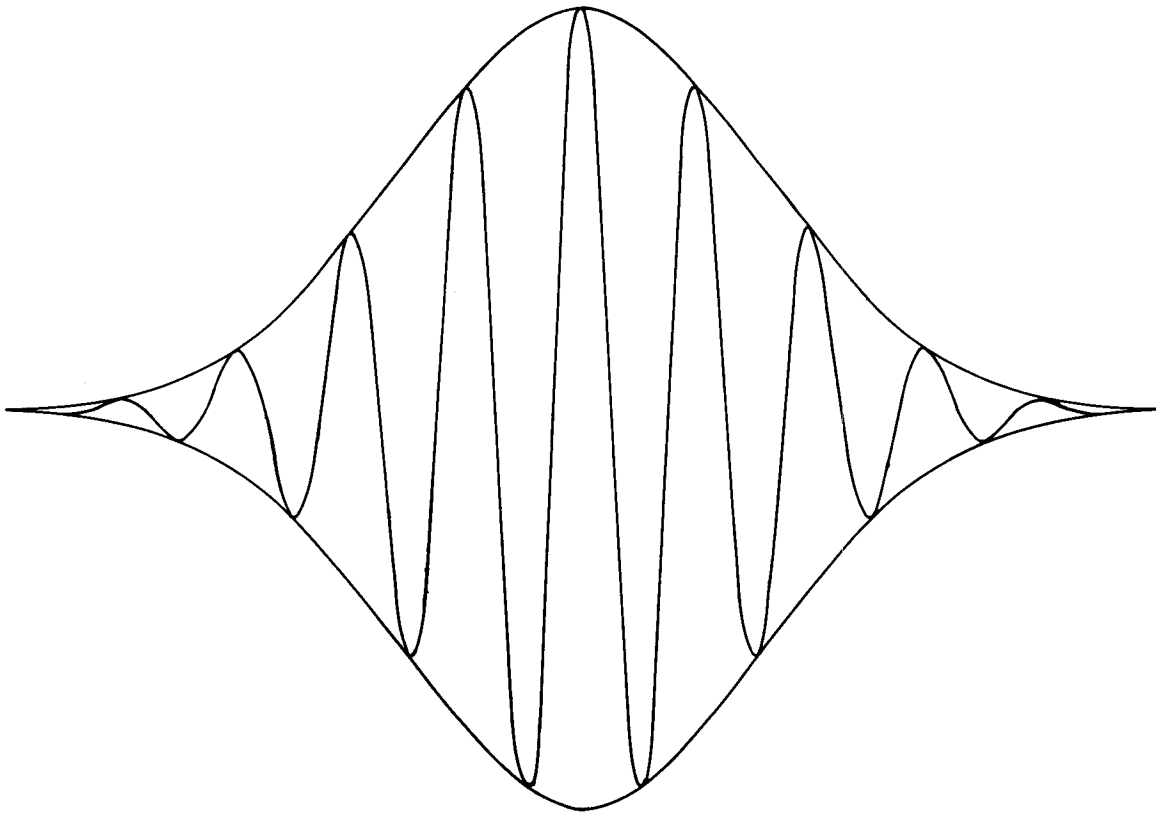


Illustration of Complex Correlation Coefficient.

Fig. 16

From (i) it is clear that the oscillation of the complex correlation coefficient is function only of D_2 , which in Booker's theory has been called h . It is then a matter of measuring this oscillation. A study of the phase correlation should therefore lead to a determination of D_2 .

The two available ways of determining h would in theory allow the validity of the hypothesis on which (39)' and C), D), F), and G) are based.

In conclusion, therefore, the modified radio star scintillation theory seems to indicate the way through which important measurements of the ionosphere, at high latitudes, can be performed.

SECTION V

PROPOSED PROGRAM OF FURTHER RESEARCH

The immediate future program of this project consists of several main aspects as follows:

1. Continued routine operation of the 223 Mc and 456 Mc phase-switch interferometers.
2. Continued analysis of phase-switch interferometer records:
 - a) by scintillation index as outlined in the present report.
 - b) for time of crossover events to attach more significance to the curves of angular deviation (Fig. 12).
3. Development of improved curcuitry for the phase-sweep interferometer.
4. Construction of similar equipment for 456 Mc.
5. After the phase-sweep equipments are operating reliably, continued analysis for mean, and extreme values of $\frac{\Delta P}{P}$ for both frequencies.
6. Investigation of the frequency dependence of $\frac{\Delta P}{P}$.
7. Investigation of digitizing the amplitude and phase data directly to allow a statistical analysis of the data itself rather than using the two-step quantized procedure as at present.

SUMMARY

This report describes the results of more than twelve months operation of the 223 Mc and 456 Mc phase-switch interferometers. The main results and conclusions reached are summarized below.

The magnitude of the 223 Mc amplitude and angular scintillations effects have been determined at an auroral latitude using two extraterrestrial radio sources. These magnitudes are discussed in terms probability distributions, mean values, and diurnal, azimuthal, elevations, and source effects.

- a) The probability of occurrence of each of the five main levels of 223 Mc scintillation activity is given.
- b) Typical amplitude probability distributions and mean values of fractional deviation in power are given for each of these indexes.
- c) Representative values of mean angular scintillation, and probability distribution for angular scintillation are given for each main 223 Mc scintillation index.
- d) The diurnal variation for both sources shows a maximum of scintillation activity at about magnetic midnight (\sim 0140 AST), with a ratio of about 1.8 to 1 between maximum and minimum. It is suggested that the activity is controlled in part by magnetic time.
- e) An azimuthal dependence has been found for the Cygnus source, which scintillates most strongly when seen towards magnetic north (some 30 degrees east of true north). It is suggested that the activity is controlled in part by the magnetic latitude at which the ionosphere is traversed.

- f) Both sources show very little variation of scintillation activity with zenith angle. (Cygnus covers the range 24 degrees zenith distance to 75 degrees, Cassiopeia 6 degrees to 57 degrees). This lack of zenith angle dependence is attributed to the elongation of the irregularities along the earth's magnetic lines of force.
- g) The scintillation activities of the two sources are different, and in particular, the zenith angle dependences are different. These differences are attributed to the larger angular subtension of the Cassiopeia source.
- h) A recent paper on the theory of radio star scintillations is modified to take into account an elongation of the ionospheric irregularities along the magnetic field lines.

Note that the occurrence of radio star fades, as observed on phase-switch and phase-sweep interferometers, has already been reported and described in Quarterly Progress Report No. 6.

REFERENCES

1. Rosson J., Cohen M. H., Radio Noise and Atmospheric Refraction at VHF and UHF, Research Report EE 351, Cornell University, Ithaca, New York.
2. Quarterly Progress Report No. 6, Contract No. AF 30(635)-2887.
3. Little C. G., Ph. D. Thesis, University of Manchester, January 1952.
4. Dagg D. M., JATP 11, 133 (139), (1957).
5. Hewish A., Proc. Roy. Soc. A 214, 494 (1952).
6. Baade W., Minkowski R., Astr. J. 119, 206, (1954).
7. Jennison R. C., Das Gupta M. K., NATURE 172, 996, (1953).
8. Booker H. G., Proc. IRE 46, 298, (1958).
9. Feinstein J., Trans. PGAP AP-2, 63, (1954).
10. Booker H. G., Ratcliff J. A. and Shinn D. H., Phil. Trans. Roy. Soc. A, 242 579, (1950).